TOKAMAK EXPERIMENTAL POWER REACTOR

W. M. STACEY, JR., M. A. ABDOU, J. N. BROOKS, I. CHARAK, R. G. CLEMMER, J. DAWSON, K. EVANS, J. A. FASOLO, R. FUJA, S. D. HARKNESS, R. L. KUSTOM, V. A. MARONI, B. MISRA, J. MOENICH, A. MORETTI, J. NOREM, W. F. PRAEG, D. L. SMITH, H. C. STEVENS, L. TURNER, S-T. WANG AND C. K. YOUNGDAHL
Fusion Power Program
Argonne National Laboratory
Argonne, Illinois 60439
United States of America

ABSTRACT. A tokamak experi ntal power reactor has been designed that is capable of producing net electric power over a wide range of possible operating conditions. A net production of 81 MW of electricity is expected from the design reference conditions that assume a value of 0.07 for beta-toroidal, a maximum toroidal magnetic field of 9 T and a thermal conversion efficiency of 30%. Impurity control is achieved through the use of a low-Z first wall coating. This approach allows a burn time of 60 seconds without the incorporation of a divertor.

The system is cooled by a dual pressurized water/steam system that could potentially provide thermal efficiencies as high as 39%. The first surface facing the plasma is a low-Z coated water cooled panel that is attached to a 20 cm thick blanket module. The vacuum boundary is removed a total of 22 cm from the plasma, thereby minimizing the amount of radiation damage in this vital component.

Consideration is given in the design to the possible use of the EPR as a materials test reactor.

It is estimated that the total system could be built for less than 550 million dollars.

1. INTRODUCTION

Three design studies [1-4] for a tokamak Experimental Power Reactor (EPR) were conducted in the USA during 1974-1976. The general objective of these studies was to define the characteristics of a net electric power producing experimental reactor that could operate in the mid- to late-1980's. The designs that evolved from these studies were, in general, characterized by relatively conservative assumptions about plasma energy confinement and β-limits and by technology extrapolations that were constrained to be consistent with the proposed operating date. The conservative β-limits (3-5%) led to rather large devices (major radii greater than 6 m) in two designs, [2,4] while the third design [3] achieved a smaller size by assuming that β of 10% could be obtained with a highly elongated (b/a = 3) doublet-shaped plasma. These studies were, to varying degrees, carried out in sufficient detail to identify the design and technological problems and to define "first-cut" design solutions. A follow-on study at ANL has concentrated on simplifications and cost reductions which can be achieved based upon more favorable β-limits predicted by recent theoretical studies and upon improved engineering design.

2. DESIGN SUMMARY

An EPR design has been developed which meets the general objectives given in Table 1. A perspective view of this design is shown in Figure 1 and a vertical section view is shown in Figure 2. The principal geometric and performance parameters are given in Table 2.

Table 1. EPR Design Objectives

- 10-50 MWe Net Electrical Power
- 1990-95 Initial Operation *
- Improved Engineering Design*
- Cost Reduction*
- Engineering and Materials Testing Capability

* Relative to previous EPR design.

Table 2. EPR Design Summary

Major radius, R(m)	4.7
Plasma radius, a(m)	1.34
Aspect ratio, A	3.5
Plasma elongation, b/a	1.65
Blanket/shield thickness (m) inner/outer	0.80/1.30
TF coil bore (m)	8.73 x 5.64
Maximum toroidal field, B_{MAX}^{TFC}(T)	10 (9*)
Average beta toroidal, β_t	0.07
Plasma current, I(MA)	7.3
Burn pulse (s)	60
Duty cycle (%)	80
Net electrical power (MWe)	81
Volt-second to plasma (V-s)	57
First-wall neutron load (MW/m^2)	0.7
First-wall lifetime (yr.)	$\geq$ 5
Tritium inventory (kg)	1.3
Reactor containment building height x diameter (m)	55 x 54
Total costs ($M)	539

* Operating reference point.

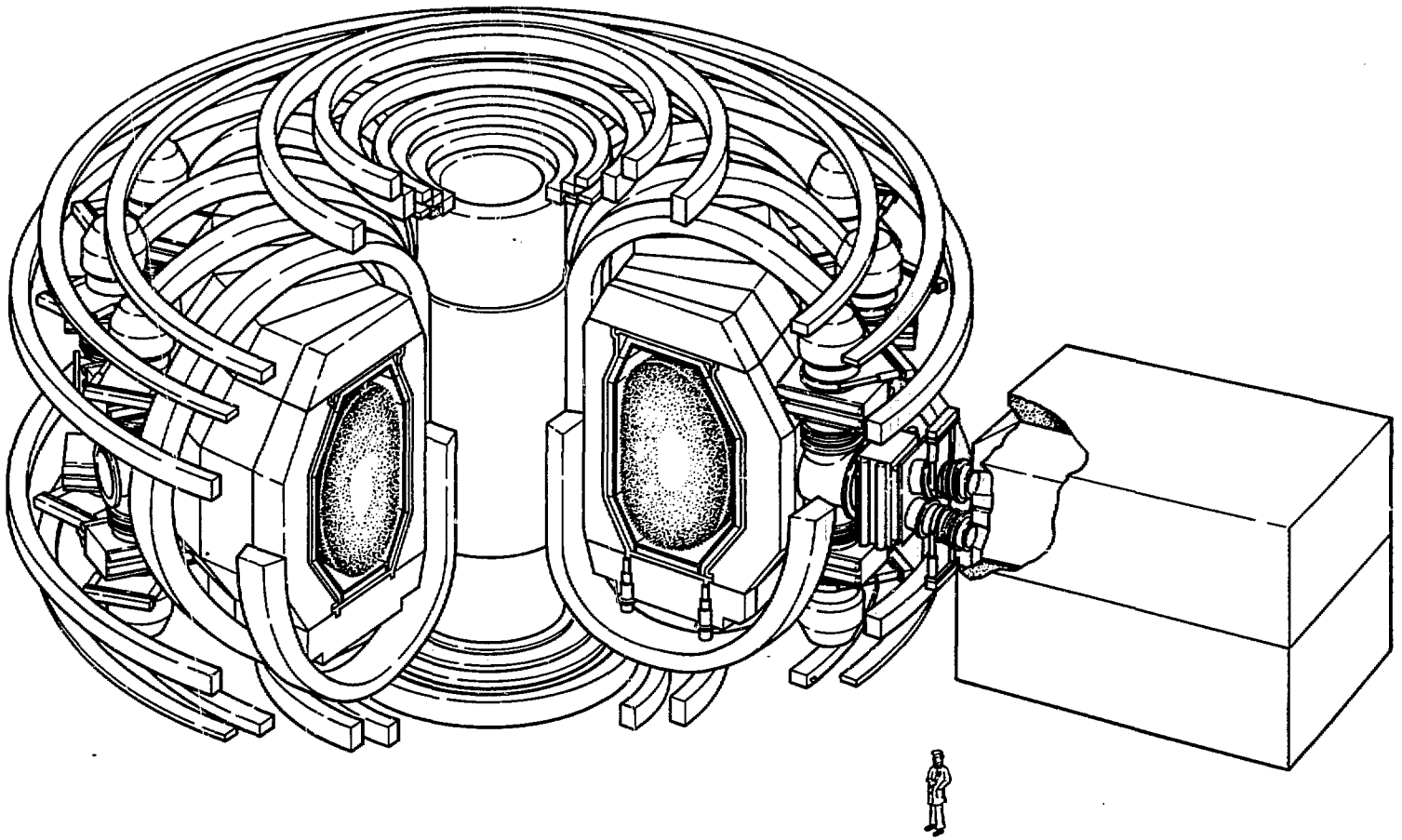

Figure 1. Perspective View of ANL EPR.

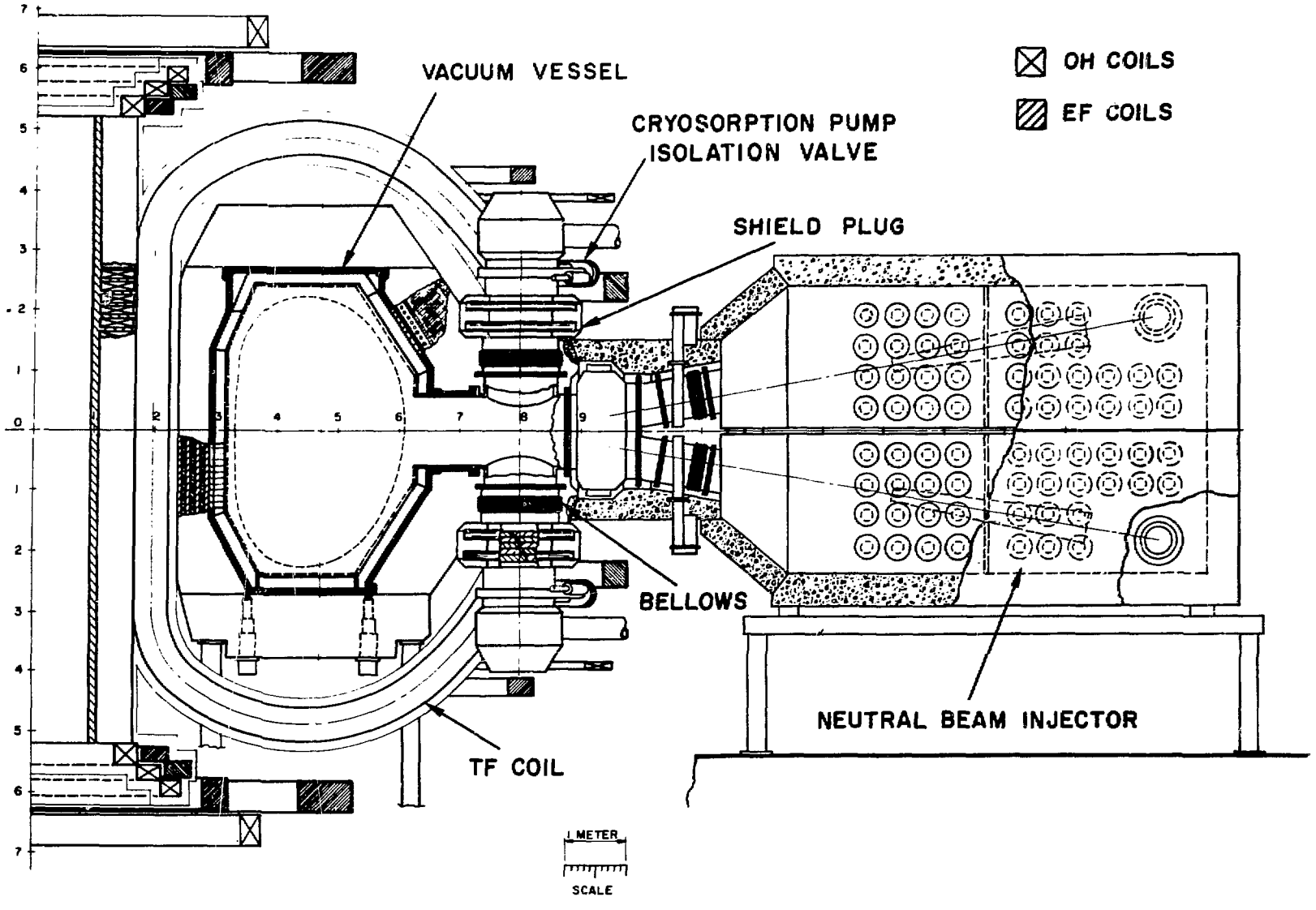

Figure 2. Vertical Elevation Showing Torus and Neutral Beam Design.

The EPR is an ignition device which uses 316 stainless steel as the structural material with energy conversion via a water/steam system. The toroidal and poloidal fields are provided by NbTi superconducting magnets. The plasma is heated to ignition by D^0 injection, although rf heating is an option. Energy is transferred into and out of a superconducting energy storage inductor to operate the poloidal coil and plasma heating systems, and a separate set of homopolar generators is used for current reversal in the ohmic heating system. A tritium system is provided which collects the reactor exhaust; separates, purifies, and enriches the fuel; and recycles it to the vacuum chamber.

3. REACTOR PHYSICS AND POWER PERFORMANCES

There is recent theoretical evidence [5-9] for the existence of MHD equilibria which support a significantly larger plasma pressure, and, hence, a larger β, than previously had been supposed. Thus, it appears that the β-limit for tokamak plasmas will be determined from MHD stability constraints.

An extensive trade-off study was performed [10] to determine the size and geometrical configuration of an EPR which would be able to produce net electrical power and achieve ignition even if confinement is as poor as is predicted by the trapped-ion-mode (TIM) theory. Two configurations were chosen for detailed study: (1) (R = 5.0 m, A = 3.0, b/a = 1.3); and (2) (R = 4.7 m, A = 3.5, b/a = 1.65). In both cases a D-shaped plasma with a shape factor (d) of 0.25 was chosen. See Table 2 for a summary of the geometric parameters for the second configuration, which was chosen as the reference.

Reasonable equilibria (i.e. those with centrally peaked current profiles no current reversal, and no excessive distortion of flux surfaces) with q(o) = 1 and q(a) = 3 were found which could support a toroidal beta, β_t, up to $\lesssim 10\%$,

for both designs. PEST code [11] calculations* indicate an upper limit of $\beta_t < 6\%$ for plasmas which can be stabilized against kink and ballooning modes; however, a number of important effects are not included in these linear stability analyses. This work led to the choice of $\beta_t = 7\%$ as the design basis for EPR, with provision for achieving the design objectives even if $\beta_t < 6\%$.

A reactor design based on the more elongated (1.65) plasma conditions was chosen as the reference point. Plasma parameters for the reference case are given in Table 3 for a range of β_t and B_{max}^{TFC} values. There are a range of design points which should achieve ignition with confinement poorer than that predicted by TIM theory (α_{TIM} is the ratio of energy confinement required for ignition, $n\tau_E = 3.4 \times 10^{20}$ s/m^3, to that predicted by TIM).

A series of burn cycle dynamic simulations were carried out in order to evaluate the cycle averaged power performance and the requirements upon the plasma driving and heating systems. For this purpose a reference plasma condition that yielded a maximum thermal power output of 606 MWth and had a maximum plasma current of 7.3 MA was chosen. Trade-off studies were performed to optimize the startup procedure. The length of the burn pulse is determined by the accumulation of impurities -- a pulse length of 60 s is felt to be achievable when a beryllium coating is used on the vacuum chamber surface, as discussed in the next section. Beam penetration calculations were performed to determine the required energy of the deuteron beam, based upon a reduced (1/5 to 1/10) density startup. The power performance parameters are summarized in Table 4, and the plasma driving and heating system requirements are specified in Table 5. The net energy flow during the burn cycle

* Performed by A. M. M. Todd, PPPL.

Table 3. Plasma Parameters for ANL EPR-77

β_t	B_{max}^{TFC} (T)	P_T (MW)	P_W (MW/m^2)	n_{DT} (10^{20} m^{-3})	I_P (MA)	α_{TIM}
0.05	8	194	0.4	0.8	6.4	1.6
	9	311	0.7	1.0	7.2	0.8
	10	474	1.0	1.2	8.0	0.4
0.06	8	279	0.6	1.0	6.4	1.1
	9	447	0.9	1.2	7.2	0.5
	10	681	1.4	1.5	8.0	0.3
	8	378	0.8	1.1	6.5	0.8
0.07*	9	606	1.3	1.4	7.3	0.4
	10	923	2.0	1.8	8.1	0.2
0.08	8	491	1.0	1.3	6.6	0.6
	9	786	1.7	1.6	7.4	0.3
	10	1200	2.5	2.0	8.2	0.2
0.09	8	619	1.3	1.5	6.7	0.5
	9	992	2.1	1.8	7.5	0.3
	10	1510	3.2	2.3	8.3	0.1
0.10	8	761	1.6	1.6	6.8	0.4
	9	1220	2.6	2.1	7.6	0.2
	10	1860	3.9	2.5	8.5	0.1

* Reference case.

Table 4. EPR Power Performance (Nominal)

Burn pulse length (s)	60
Dwell time (s)	15
Fusion energy/pulse (GJth)	23.4
Gross electrical power (MWe)	117
Net electrical power (MWe)	81

Table 5. EPR Plasma Driving and Heating System Requirements for Complete Burn Pulse

Volt-second to plasma (V-s)	57.0
Magnetic Energy (GJ)	2.7
OHC current reversal time (s)	2
Maximum field in OHC (T)	5.7
Maximum field rise in OHC (T/s)	6.7
Auxiliary heating power (MW)	40
Auxiliary heating time (s)	4.1
Neutral beam energy (keV)	180

is indicated in Figure 3. The reference operating point for the above mentioned calculations is β_t = 7% and B_{max}^{TFC} = 9T and assumes a thermal to electrical conversion efficiency, ε_{TH}, of 0.30.

Figure 4 shows the variation in the net electrical power, for a 60 s burn cycle, for different values of the principal parameters. There is clearly a wide range of β_t-B_{max}^{TFC}-ε_{TH} for which this design would meet the power performance requirements for an EPR.

4. IMPURITY CONTROL

A passive impurity control measure -- coating the vacuum chamber wall with a low-Z material -- is proposed for EPR. The net electrical power averaged over the burn pulse has been computed [12] as a function of the surface material and the length of the burn pulse, the latter being determined by the accumulation of impurities. With a bare stainless steel wall, the plasma was quenched immediately upon the termination of auxiliary heating, and the net electrical power was a negative value of several hundred megawatts.

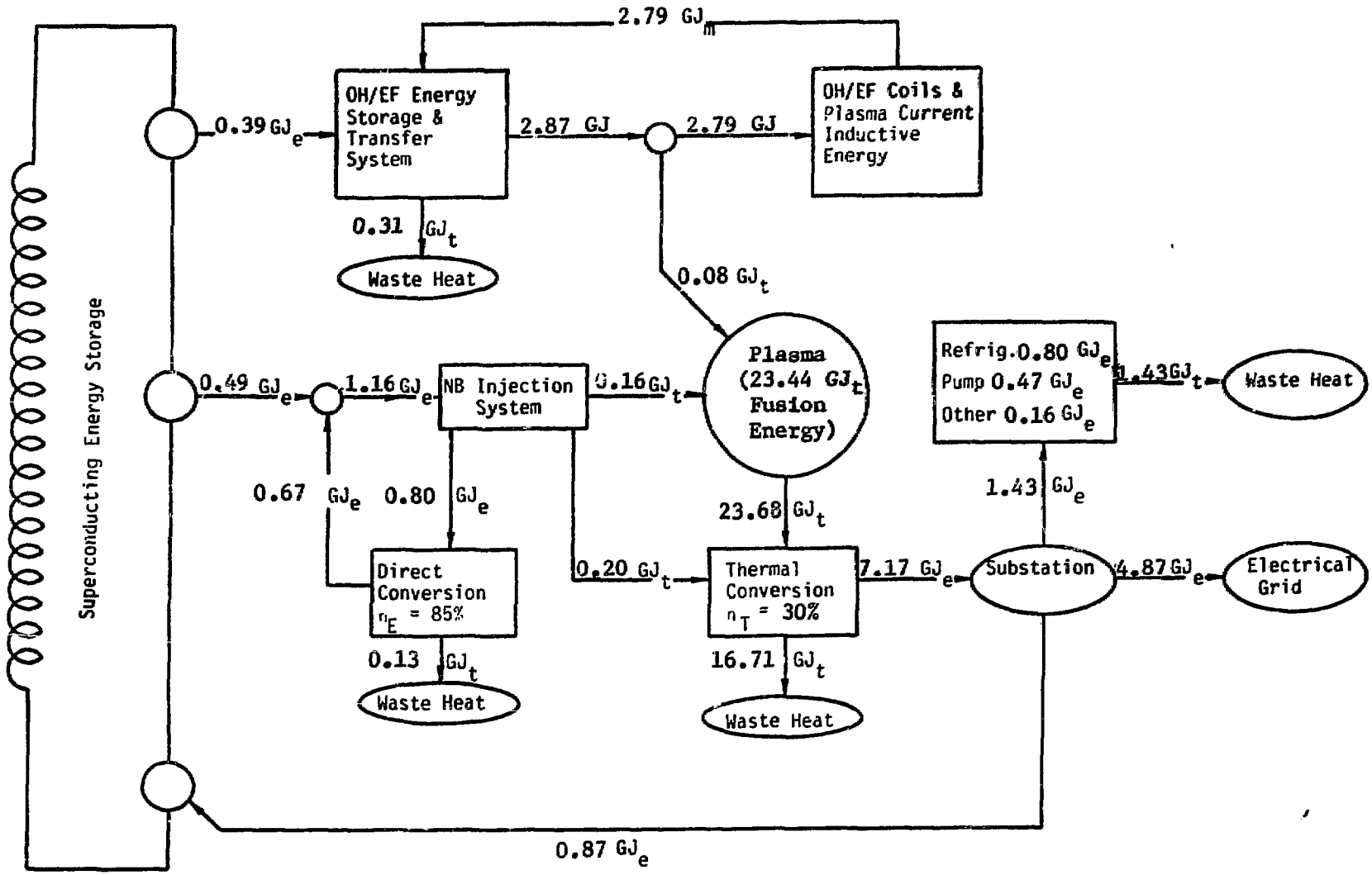

Figure 3. Net Energy Flow in Reference Burn Cycle.

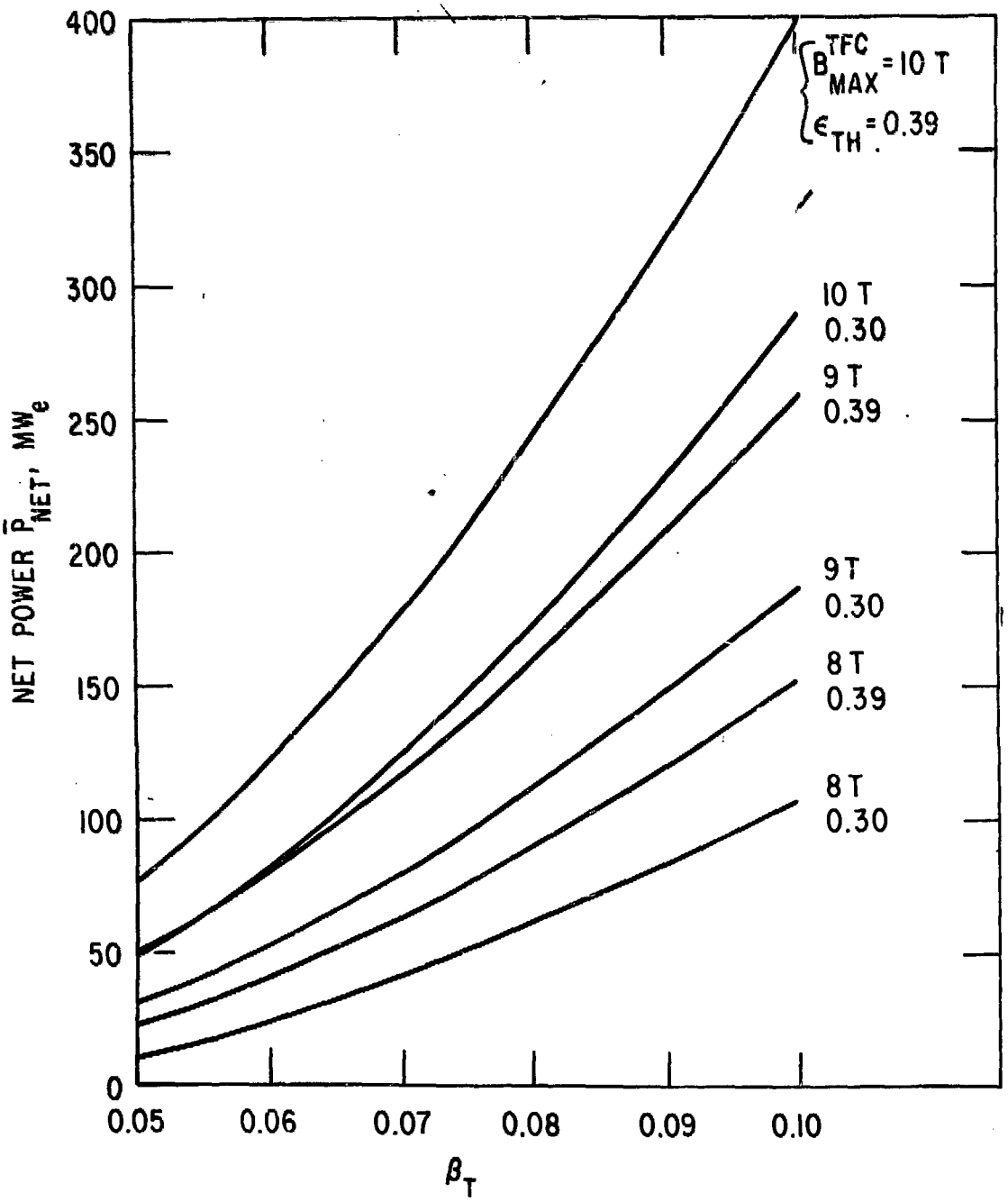

Figure 4. Net Electrical Power Production as a Function of β_t, Toroidal Magnetic Field and Thermal Conversion Efficiency.

Calculations indicate that coating the first wall with a low-Z material will provide sufficient impurity control for the operation of an EPR. It is concluded that a ∿ 1-2 minute burn pulse and net electrical power production is possible in an EPR using a low-Z coating for impurity control.

5. PLASMA HEATING SYSTEMS

A number of different alternatives are being considered for heating the EPR plasma from breakdown to ignition. These methods must be capable of producing 40 MW of power for about 4 to 6 seconds in order to heat the plasma to ignition. The most promising alternatives are neutral beam and radio frequency (rf) heating, with neutral beams presently considered to be the primary option.

Detailed designs of several neutral beam injector systems which would be applicable to a large machine have been developed. Three options, requiring varying degrees of extrapolation beyond the state of the art for TFTR ion sources, are summarized in Table 6. Two of the options assume the use of positive deuterium ion sources with D^+ fractions of 75 and 95 percent, respectively; these designs may be regarded as lower and upper limits to what might be achieved with sources of positive deuterium ions. Design 1 is the current reference. Design 2 represents a worthy but perhaps not quite attainable goal for further ion source development work. The third option is based on the possibility that a suitable extraction D^- ion source will be developed for the next generation of machines. To produce the monoenergetic neutral beams required by these machines from a beam consisting initially of positive atomic and molecular deuterium ions, we consider a basic system of an ion source that produces a diverging beam followed by a double focusing D^+

Table 6. 40 MW Neutral Beam Injection System for Tokamak EPR

	Design 1	Design 2	Design 3
Atomic ion*	180 keV D^+	180 keV D^+	400 keV D^-
Beam composition (D^+, D_2^+, D_3^+)	(0.75, 0.18, 0.07)	(0.95, 0.03, 0.02)	95% D^- Assumed
Target For $D^+ \rightarrow D^0$	D gas	D gas	D gas
Number of injectors	12	12	12
Number of ion sources/injector	2	2	2
Ion beam current density (A/cm^2)	0.135 avg.	0.135 avg.	0.080 avg.
Ion beam power (MW)	261	204	76
Source gas efficiency	0.45	0.50	0.10
Gas load/injector (Torr-ℓ/s)	70.4	41.8	15.3
Pumping speed/injector (ℓ/s)	4.2×10^6	4.0×10^6	2.6×10^5
Zr-Al panel area/injector** (m^2)	126	120	8
Electrical power effi ency	0.33	0.44	0.65
Overall power efficiency***	0.38	0.48	0.70
Net power input (MW)	121	91	62

* Circular, initially diverging D^+ beam; square, initially converging D^- beam.

** The required area has been doubled to allow for regeneration.

*** Assumes direct conversion efficiency = 0.85, thermal conversion efficiency = 0.30.

bending magnet, a tapered neutralizer, a second bending magnet and direct energy convertors to recover energy from unused molecular and atomic ions. Zirconium-aluminum getter pumps are presently planned for all systems because of their relative insensitivity to neutron bombardment and their ability to operate at elevated temperatures.

A system to deliver 40 MW of ion-cyclotron heating (ICRH) using ridged waveguides is under study. The guide should be capable of delivering 2.5 MW to the plasma at 58.5 MHz. Sixteen of these would be required to deliver 40 MW. The waveguide could be coupled to a 9-inch coaxial cable inside the outer blanket. Any system used in an EPR must be relatively simple, rugged, efficient and flexible enough to follow changes in density, temperature and major and minor radii. The radiation environment also imposes severe constraints.

The lower-hybrid heating (LHRH) system plan would be similar to that proposed in the previous design [2]. A phased array, the Lallia-Brambilla "Grill", [1] of reduced height, WR 510 waveguide is under study. This may allow plasma to be heated at a frequency of around twice the lower hybrid resonance value, which would avoid power limitations caused by parametric instabilities [2].

6. ENERGY STORAGE AND TRANSFER

The energy storage and transfer (EST) system consists of a central energy storage inductor (ESI), a thyristor bridge system to transfer energy between the ESI and the OH coil, EF coil and neutral beam (or rf) systems, and a rectifier to transfer makeup energy from a power substation into the ESI.

A separate inertial energy storage unit, consisting of radial-stacked homopolar generators, is used to transfer inductive energy into and out of the OH coil system. The EST design requirements were determined from burn cycle simulations, as discussed in Section 3. The EST system is summarized in Table 7 and described in more detail in Reference 2.

6.1 Ohmic Heating System

The conceptual design for the EST device for the OH coil is based on using counter cyclonic generator (CCG) type homopolar generators with NbTi coils in a magnetic yoke [2]. Ten modules in series will develop 51,300 volts and will have a minimum capacitance of 0.523 farads. The minimum field reversal time in the absence of stray inductances and circuit losses would be 1.92 s.

The CCG is disconnected from the OH coil during the burn. The OH coil current and $\dot{B}$ are maintained with a separate power supply driven from a central energy storage inductor. An actively controlled inductor-convertor of the type described for the EF coils is used for this application. A total of 490 MJ is taken from the ESI during the burn. The inductor-convertor will provide a peak voltage of 800 V and the energy transfer is reversible.

6.2 Equilibrium Field System

An actively controlled version of an inductor-convertor bridge [13,14] driven from a central ESI is selected as the power supply and energy storage choice. A circuit diagram for a 3-phase inductor-convertor bridge is shown in Figure 5. The EF coil is represented by L_E and the central energy storage coil is represented by L_S. The capacitors in the circuit are relatively small in the sense that they only store a small fraction of the total magnetic energy in the circuit. The left-hand (LH) bridge commutates the L_S current

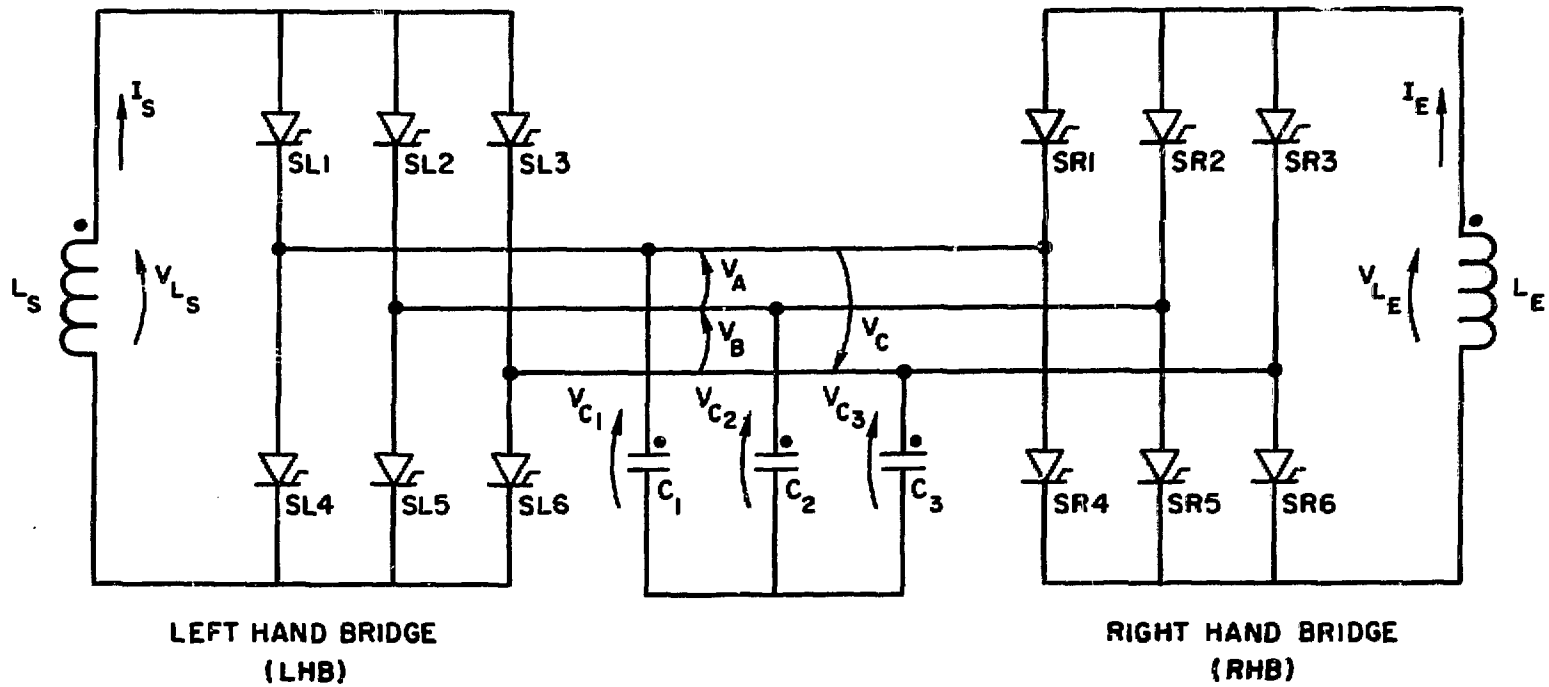

Figure 5. Inductor-Convertor Bridge Circuit Diagram for Equilibrium-Field Coil System.

Table 7. Energy Storage and Transfer Systems - Maximum Ratings for Reference Burn Cycle

Ohmic Heating Systems

Homopolar Generators

No. of generators in series	10
No. of drums per generation	8
Total energy transfer (MJ)	607
Peak power (MW)	957
Peak available voltage (kV)	51.3
Peak available current (kA)	41.1
Minimum equivalent capacitance (f)	0.523

Rectifier System

Type	3 Ø inductor-convertor bridge
Energy transfer (MJ)	490
Peak power (MW)	56
Peak current (kA)	70
Peak voltage (kV)	0.8
Switching frequency (Hz)	100

Equilibrium Field System

Type	3 Ø inductor-convertor bridge
Energy transfer (MJ)	1770
Peak power (MW)	448
Peak current (kA)	70
Peak available voltage (kV)	26
Switching frequency (Hz)	100

Neutral Beam System

Type	SCR, DC/AC/DC at kHz
Energy transfer (MJ)	480
Voltage (kV)	180
Power (MW)	120

Central Energy Storage Inductor

Type	Superconducting ring dipole
Energy stored (MJ)	3700
Energy transfer (MJ)	2750
Peak current (kA)	70
Peak power (MW)	570
Average power from utility grid or power plant (MW)	10.7

through the three capacitors so as to create cyclic voltages on each capacitor, which are separated 120° in phase from each other. The right-hand (RH) bridge is switched in the same sequence but at a different relative time from the OH bridge. The current in L_E affects the voltage waveshape on the capacitors. The peak voltage required for normal charging of the EF coil is 18,500 V. The bridge is designed to operate with a switching frequency on the right hand bridge leading the left hand bridge by 45° when 18,500 volts is generated across the EF coil. The phase can be advanced to 90° to generate 26 kilovolts across the EF coil or phased back to where -26 kilovolts can be generated.

6.3 Neutral Beam Power Supply

The neutral beam injector energy transfer system is composed of two major components; a saturated time-delay transformer (STDT), [15] which uses the saturation effects of magnetic cores to act as a current surge limiter, and a high frequency, polyphase-controlled rectifier [16] using SCR switches to enable rapid de-energization of the beam in periods of less than 100 μs. A circuit diagram is shown in Figure 6.

The injector power supply extracts energy from the same central ESI that the EF coil power supply uses. An inductor-convertor similar to that described for the EF coil system drives a high frequency, polyphase invertor. A 10 kHz voltage is developed in a summing transformer, filtered and subsequently rectified. The output lead is connected to the injector through an STDT. In the event of a spark, the STDT prevents energy transfer into the spark and, if necessary, the polyphase rectifier can be phased back quickly enough to remove power from the injector in the event that the discharge path has not cleared in a time beyond which the STDT is unable to absorb the energy.

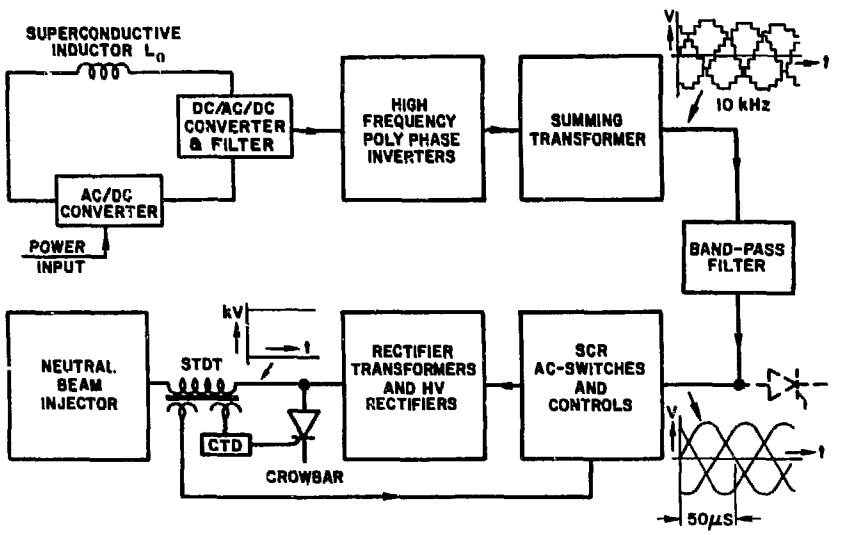

Figure 6. HV Power Supply for NBI Block Diagram.

Nonsaturated, longitudinal reactors [17] limit the discharge current of the energy stored in the circuit capacitance of the filament and of the arc power supplies.

6.4 Central Energy Storage Inductor

The neutral beam injector and/or rf amplifier power supplies and EF and OH coil power supplies extract energy from a central energy storage inductor (ESI). The ESI is a superconducting ring dipole (torus) with a minor radius of 0.8 m, a major radius of 3.9 m, a peak field of 5 T and an inductance of 1.51 h. The design of the conductor for the ESI is based on the Rutherford cable concept with 200 1-mm diameter wires wound on an 0.003 m by 0.097 m fiberglass support strip. The conductors would be the same as those developed for the poloidal coil design. A rectifier power supply draws an average power of 10.7 MW from the substation to resupply losses in the energy storage and transfer system.

7. MAGNETS

The toroidal and poloidal field coil systems are summarized in this section. These systems are described in Reference 16.

7.1 Toroidal Field Coils

The superconducting toroidal-field (TF) coil parameters are given in Table 8. The TF coils are designed for nominal operation at 9 T and 4.2 K, but with provision to operate at 10 T by pumping down to 3.7 K in order to compensate if β is lower than is anticipated.

The TF coils are designed for cryogenic stability. Because most of the resistivity of the copper stabilizer is magnetoresistivity and radiation-induced

Table 8. Toroidal Field Coil Parameters

Number of coils	16
Coil shape	Pure-tension D
Superconductor	NbTi
Stabilizer	Copper
Support material	Stainless steel
Support cylinder	Fiberglass-reinforced plastic
Coil bore, vertical x horizontal	8.73 m x 5.64 m
Allowed stress in copper and SC	15,000 psi
Allowed stress in stainless steel	60,000 psi
Operating temperature	3.7 K (4.2 K)
Peak field	10 T (9 T)
Field at plasma	4.81 T (4.33 T)
Total amp-turns	115 MA-turns (104 MA turns)
Operating current	60,000 A (54,000 A)
Turns per coil	60 x 2
Average current density	1540 A/cm^2 (1386 A/cm^2)
Inductance	7.9 Henry
Stored energy	14.3 GJ (11.6 GJ)
Weight of NbTi	43 Mg
Weight of copper	552 Mg
Weight of stainless steel	328 Mg

resistivity, both of which vary across the coil, the copper is graded with more copper on the inner turns where the radiation level and magnetic field are largest. The NbTi is also graded; less is required on the outer turns where the field is lower and the critical current density is higher. A 50 kA sheet conductor is specified, consisting of a sheet of copper with NbTi-copper composite wires stranded around it and soldered to it. Stainless steel reinforcement is wound with the sheet conductor into two pancakes per coil with a support rib between them. The conductor is wound in precompression and the stainless steel in pretension so that the stainless steel will support 60,000 psi tensile stress without stressing the copper beyond 15,000 psi when the coils are energized. Such a conductor is inherently a dc conductor and is enclosed by a high-purity aluminum field shield operating at 18 K to reduce the ac losses from the pulsed plasma and equilibrium fields.

The TF coils operate in series to eliminate the possibility of carrying unequal currents, which would produce large bending moments and out-of-plane forces at the coils. Protection circuitry includes a dump resistor which is always connected. A surge in magnet terminal voltage in any coil due to a normal region developing will serve as a signal to disconnect the power supply. The dump resistor is sized to prevent the development of excessive voltage during the discharge.

7.2 Poloidal Field Coils

The ohmic-heating (OH) and equilibrium-field (EF) coils are located external to the TF coils to facilitate installation and maintenance and to allow them to be superconducting. The location of these coils is shown in Figure 2, and the principal parameters are given in Table 9.

Table 9. Poloidal Coil Parameters at Maximum Design Ratings

	OH Coils	EF Coils
Number of coils	Solenoid + 10	12
Location	Outside TF coils	Outside TF coils
Superconductor/Stabilizer	NbTi/Cu	NbTi/Cu
Operating temperature	4.2 K	4.2 K
Current density	1730 A/cm^2	1730 A/cm^2
Operating current	70 kA	70 kA
Total amp-turns	82.3 MA turns	54.4 MA turns
Maximum Volt-seconds	90 V-s	37 V-s
Central field	8 T	0.3 T
Maximum rate of change of field	6.7 T/S	---
Field at plasma	$< 10^{-3}$ T	0.56 T
Inductance	0.73 H	0.94
Coupling coefficient to plasma	- 0.25	- 0.175
Self inductive energy	1.75 GJ	2.3 GJ
Inductive energy: OH & EF and plasma	3.7 GJ	

The OH coils consist of a central solenoid and ten additional coaxial coils. The central solenoid is between the TF coils and the central support cylinder; it is interrupted every 25 cm axially by a 5-cm high steel ring which transmits the TF coil centering force to the fiberglass-reinforced plastic support cylinder. This configuration maximizes the central flux core area for a solenoidal OH coil that provides the necessary volt-seconds. The OH coils are energized to give a negative flux before the plasma is formed, then the current in the OH coils is reversed, inducing a current in the plasma.

The EF coils are decoupled magnetically from the OH coils by locating them all on the same flux line of the OH coils, operating them in series, and requiring that the numbers of positive and negative amp-turns in the EF coil system be equal. Selection of the flux line and of the coil positions along the flux line are governed by engineering constraints. The currents are selected so as to establish the required equilibrium field configuration in the plasma, using a free-boundary MHD equilibrium code, but subject to the constraint of minimizing energy in the EF coil system. The required field pattern could be achieved for plasma shape factors (d) of 0.25, but not for d = 0.5, with the EF coils excluded from the central flux core and located externally to the TF coils.

The EF and OH coils are cryogenically stable. A 70 kA fully-transposed cable of copper and superconducting composite strands around a stainless steel solid or stranded stip is specified. This design is described in Reference 2.

A system of water-cooled copper coils is located within the blanket and shield. This coil system provides the ∿ 500 V, 5 ms voltage pulse necessary to break down the plasma and also provides the trimming fields necessary to control the plasma position.

8. FIRST WALL/BLANKET/SHIELD AND ENERGY CONVERSION SYSTEMS

The basic features of the present design point for the first wall/blanket/shield (FW/B/S) are illustrated in Figure 7, summarized in Table 10 and described in more detail in References 19 and 20. The vacuum vessel is an irregular toroidal shell, fabricated from 7-cm thick stainless steel plates that are welded together in sections. This shell forms the primary vacuum boundary for the plasma chamber, is located outside the blanket assembly and

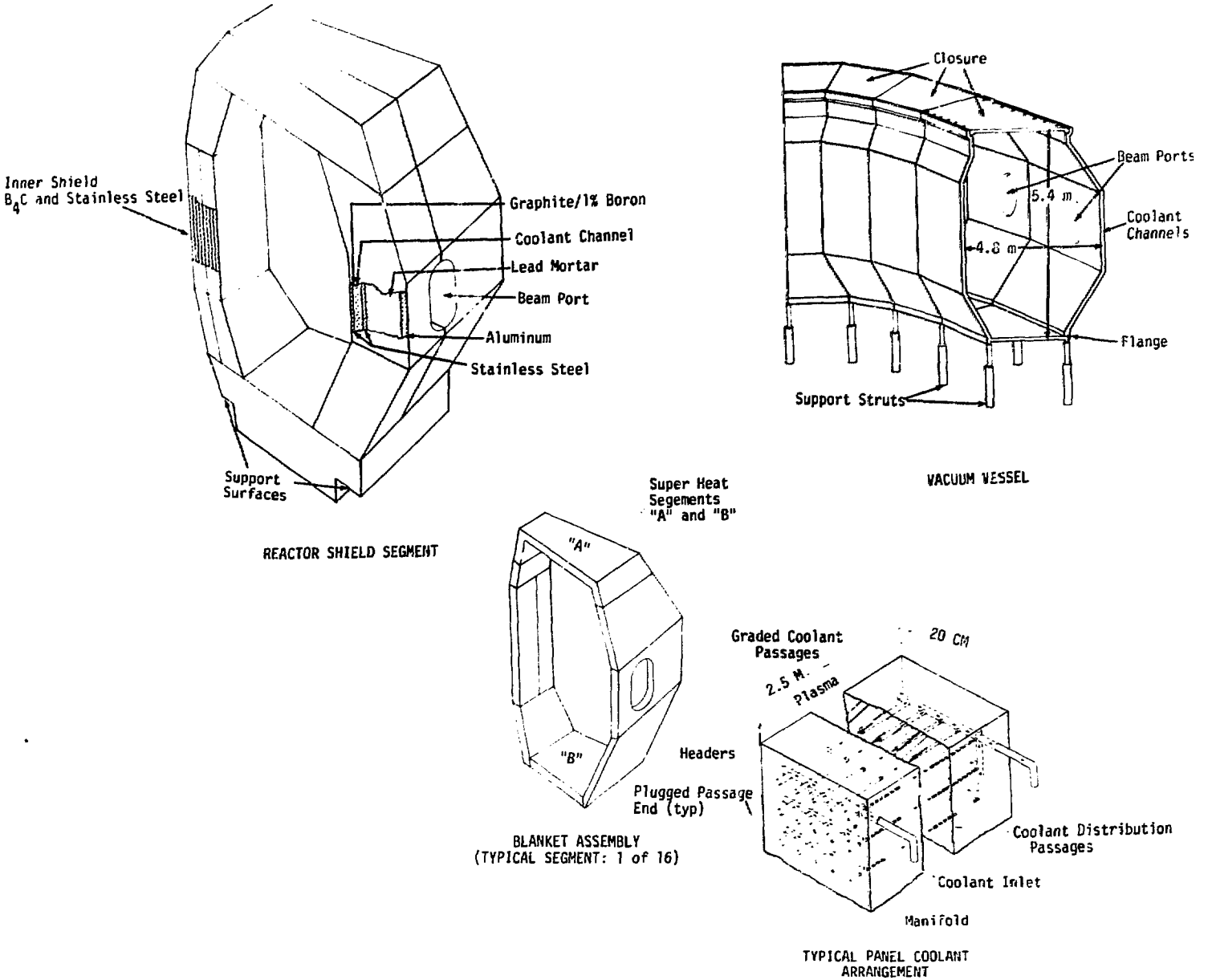

Figure 7. Design of Segmented Blanket, Vacuum Vessel and Shield Components.

Table 10. Major Design Concepts and Parameters for the EPR First Wall/Blanket/Shield System

First Wall	
Type	Cooling panel
Thickness	1–2 cm
Material	316 SS, BeO coated
Maximum temperature	450°C
Neutron damage	11 dpa/(MW-yr/m^2)
Helium generation	208 appm/(MW-yr/m^2)
Hydrogen generation	512 appm/(MW-yr/m^2)
Nuclear heating	7.6 W/cm^3
Neutron Wall Load	0.7 MW/m^2
Blanket	
Type	stacked rectangular slabs
Material	316 SS
Thickness	0.2 m
Coolants	pressurized H_2O/steam
Maximum temperature	550°C
Maximum nuclear heating	6.2 W/cm^3
Weight	∿ 700 Mg
Vacuum Vessel	
Type	modular sections, welded plate
Location	outside blanket
Number of sections	16
Number of plates/section	12
Material	316 SS
Dimensions	
Thickness	0.07 m
Vertical bore	5.4 m
Horizontal bore	3.1 m
Section semiangle	22.5°
Maximum temperature	550°C
Coolant	pressurized H_2O
Coolant geometry	gun-bored channels
Weight	∿ 260 Mg
Heating Rate	1.0 W/cm^3
Bulk Shield	
Material	
inner	304 SS, B_4C
outer	B, C, Pb-mortar, 304 SS, Al
Thickness	
inner	0.52 m
outer	1.0 m
Weight	∿ 2000 Mg
Maximum nuclear heating	0.55 W/cm^3

provides the principal support for that assembly. The section shown in Figure 7 is one of sixteen which join together by bolting and seam welding to form the complete torus enclosure. The entire vacuum vessel is supported from below the reactor and is anchored to the lower (bottom) shield blocks. The top plates of each vacuum vessel section are removable and provide the access for all operations internal to the vessel. This large, relatively unobstructed aperture provides for simple remote operated tools and machines to be used in removal and replacement operations. All liners, blanket blocks and other internals are removed through the top closure with simple hoists and guide frames. Each vacuum vessel plate is fabricated with appropriately dispersed, gun-bored coolant channels that terminate with connections to the coolant mainfold system. By locating the vacuum vessel outside the blanket and, hence, in a zone of lower radiation exposure and reduced thermal energy generation, it becomes more accessible (e.g. for leak repair), will have longer lifetime, requires less (8 MW) cooling capacity and is in a region considerably less subject to thermal fatigue than the region inside the blanket.

The blanket assembly is comprised of stainless steel blocks with transverse gun-bored coolant channels. There are a total of 8 blocks per vacuum vessel section (supported by the vacuum vessel) which are installed and removed through the upper vacuum vessel closure.

The EPR power conversion system incorporates a dual cycle in which an indirect pressurized water system is coupled to a direct cycle superheated steam system. Pressurized water from the first wall assembly and the inner and outer blanket regions delivers thermal energy to an evaporator operating at 340°C and 13.8 MPa (2-00 psi) and utilizing much of the same technology and conditions as are presently employed in pressurized water reactors (PWRs). The

steam generated in the evaporator is fed to the upper and lower (superheater) blanket blocks where is is heated to 410°C at ∿ 8.6 MPa (1250 psi). This steam is fed directly to the turbo-generator in a fashion comparable to boiling water reactors (BWRs) and results in an overall cycle efficiency of ∿ 39%. The difficulties associated with the use of a direct cycle steam, (stemming mainly from radioactivity transport) need to be more carefully analyzed, but with the exception of a potentially higher tritium level they do not appear to be more severe than those encountered in BWRs. The principal features of this dual cycle energy conversion system are summarized in Table 11.

Table 11. EPR Energy Conversion System

Heat Transport System		
Capacity	360 MWth	
Pressurized Water Circuit		
Pressure	15.2 MPa	(2200 psi)
Inlet Temperature	238°C	(460°F)
Outlet Temperature	340°C	(644°F)
Steam Circuit		
Pressure	8.2 MPa	(1200 psi)
Inlet Temperature	300°C	(535°F)
Outlet Temperature	410°C	(770°F)
Power Plant Rating	120 MWe	(270 MWth)
Cooling Tower Capacity	315 MWth	

Thermomechanical analyses [21] of the blanket blocks have shown that pressurized water, helium and steam would all be satisfactory coolants for near-term operating scenarios. By properly grading the length and size distribution of the coolant channels in the blanket block, it is possible to

achieve realistic performance parameters (in terms of present day technology) for each of these coolants and to maintain stress levels within the blanket blocks at values that correspond to a strain of less than 0.2%. Because of the large thermal inertia of the blanket blocks, the cyclic strain variation is insignificant during normal reactor operation. The overall unconstrained thermal deformation of each block is $\sim$ 0.6% of the room-temperature dimensions with the blocks tending to become convex toward the plasma. Blanket coolant temperature drops of $< 1°C/s$ are experienced during the dwell time.

A high-performance water-cooled stainless steel panel, which is attached to the plasma side of each blanket block, serves as the first wall for the reference design. These coolant panels are designed to accept the high surface heating (equivalent to $\sim$ 25% of the neutron wall load) produced by particle transport and electromagnetic radiation from the plasma. The plasma-side surfaces of the panel walls are coated with a low-Z material, e.g., Be, BeO, or B_4C, to control the influx of high-Z transition-metal impurities into the plasma from the steel panels. Cyclic thermal stresses in the coolant panel are minimized by restricting the plasma-side panel wall to thicknesses < 0.25 cm. Calculations [22] of the thermal response of the first wall during off-normal operation indicate that the panel wall will withstand several plasma dumps if the plasma energy is evenly distributed over $\geq$ 10% of the wall (for a plasma with a nominal 1 MW/m^2 neutron wall load). A plasma dump of this type will vaporize or ablate a 5-20 μm layer of the coating, depending on the material, from the wall. Much of the vaporized material is expected to redeposit on the wall during cooling after the dump. The frequency with which a 200-μm thick coating would have to be replaced would be determined by the uniformity of the redeposition and the probability of dumps occurring on the same area of the wall.

The severe constraints on space in the high field regions of small-size reactors has been resolved for the EPR by segmenting the bulk shield into inner and outer regions that employ different shield materials. In all, there are 12 shield blocks per vacuum vessel section. All of the blanket and bulk shield blocks are electrically insulated from one another to provide the required [2] disruption of eddy currents generated by the pulsed magnetic fields. The inner blanket/shield design evolved from an extensive parametric study [23,24] including radiation effects, local nuclear heating and refrigeration power requirements in the superconducting TF magnets. Based on this study: (1) the inner shield composition is an optimized combination of stainless steel and boron carbide, and (2) the inner blanket/shield thickness is set at 0.9 m. The TF coils would be annealed at the end of each 1 MW-yr/m^2 irradiation period with the maximum radiation induced resistivity in the copper stabilizer reaching 4.2×10^{-8} Ω-cm and with only ∿ 3% change in the critical current density of NbTi. The maximum radiation dose to the epoxy insulators inside the conductor is 4×10^9 rad after 4 MW-yr/m^2 of operation. Low temperature irradiation measurements on organic insulators are required to provide a definitive radiation damage limit.

Effective shielding is provided for all penetrations that have to be accommodated in the blanket/bulk shield. The neutral beam ducts are surrounded by an 0.8-m thick local penetration shield as they emerge from the bulk shield. This penetration shield extends to the beam injectors and is tapered off in proportion with the radiation attenuation. Movable shield plugs are used where necessary to block penetrations that need not be open during the plasma burn. The concept of connecting the torus evacuation ducts to the neutral beam ducts at locations outside the blanket has been adopted because it offers

several advantages over the use of separate torus evacuation ducts that extend directly to the first wall.

9. MATERIALS

It appears at this time that there are no materials limitations that preclude the viability of the EPR design. This is in part due to the fact that a conscious effort has been made in the design to remove the vacuum vessel from the high damage region and to allow remote repairs to be made in a straight-forward manner. The relative amounts of damage expected in the different structural components are presented in Table 10.

The most vulnerable component in the EPR is the first wall cooling panel which is subjected to the highest fatigue loading while enduring the most intense radiation damage. In predicting the lifetime of this component, swelling, ductility loss and fatigue were considered. The operating temperature is an important factor in assessing all three of these areas. For example, in the temperature regime of 300 to 500°C, the form of radiation damage changes dramatically, going from a high concentration of very small point defect clusters at 300°C to an array of relatively large faulted dislocation loops and voids at 500°C. Assuming an allowable swelling of 10% and a reduction of ductility to 0.5% uniform strain, the region of the wall at temperatures in excess of 400°C would be limited to approximately 4 MW-yr/m^2 of service. Thus, based on these considerations at the nominal* EPR wall loading of 0.7 MW/m^2 and plant factor of 50%, the first wall coolant panels would require replacement every 11.4 years. Defining the lifetime of the

* The maximum wall load is 1.3 MW/m^2, but the average wall load over the burn pulse is 0.7 MW/m^2.

regions at temperatures near 300°C is more difficult, as considerably less information is available. The two properties that need better definition at this irradiation temperature are ductility and fatigue. The design limit of 0.5% uniform ductility is based upon fission reactor data. There are several factors that could cause a higher limit to ultimately be set for EPR. A more conservative limit of 1% ductility would correspond to 2.5 MW-yr/m^2, which would require wall replacement every 7.8 years. A fatigue analysis of the front coolant panels indicates that if the irradiated properties are at least the same as are currently assumed by the ASME code for 316 stainless steel then the lifetime of this component will be limited to 5 years.

There are several other areas of concern relating to the ability of different components to perform for long periods in the EPR environment. More experimental results are needed in each of the following areas before an EPR can be confidently designed.

1. Fusion welds lead to compositional and microstructural variations that could have important effects on the resistance of austenitic stainless steels to radiation damage. The extent of this problem can only be determined by experimental studies that involve the irradiation of prototypic welded samples in mixed spectrum fission reactors where the expected helium/dpa generation rates can be duplicated.
2. Another area concerns the radiation damage of high temperature inorganic insulators, since the EPR design includes a ceramic circuit breaker in the first wall. While yttria-based materials look very attractive for this application at this time, much more needs to be done to develop the necessary property data before an accurate estimate of an expected lifetime can be established.

Existing information does indicate that the yttria is stable to at least 2 MW-yr/m^2, or 6.25 years of EPR service.

3. The third area where improved information would help is in the selection of a cryogenic insulator for use in the superconducting magnets. Commonly used organic insulators may be limited to $\sim 10^9$ rads of exposure, which dictates the use of a thicker than otherwise optimum blanket and shield. More detailed information is needed on conventional glass-bonded epoxy insulators as well as on attractive alternates such as glass-bonded mica.

4. The fourth area concerns the development of a low-Z first-wall coating that either is long-lived or can be easily replaced. Sputtering rates, especially at lower projective energies, for both deuterium and helium are needed before the burn cycle can be fully defined.

Considerations of the potential materials limitations for the EPR highlights the need of the fusion program for a large capacity test facility. The EPR could fulfill this function, as several million cubic centimeters of test volume could be made available for use. At a wall loading of 1 MW/m^2 and a 50% plant factor, quantities of test specimens sufficient to statistically document the response of a wide variety of materials to a fusion environment could be exposed at the rate of about 6 dpa per year. The potential for higher wall loadings is included in the current design. Upon comparison of the EPR with other possible test facilities, one is immediately struck by the limitation of the (D,Li) and jet sources to benchmarking experiments due to their very limited experimental volume (hundreds of cc's) and the restriction of mixed spectrum fission reactors such as ORR to the testing

of nickel containing alloys. It is therefore reasonable that the EPR be used as an instrumented materials test facility.

10. TRITIUM SYSTEMS

The technical basis for the design of the EPR tritium handling systems has been described in previous publications [2,10,25,26]. In essence, these systems must provide for: (1) recycle and processing of the plasma exhaust, (2) recovery and consolidation of tritiated wastes, and (3) emergency air handling and detritiation of the reactor building and other major facility enclosures. A key attribute of the design is provision for multiple levels of containment around all components and hardware that contact sizeable quantities of tritium. This section describes the principal features of the EPR tritium facility.

A layout of the tritium handling and fuel processing facility for a near-term tokamak reactor like the EPR is illustrated schematically in Figure 8. Unburned DT fuel plus impurities collected by the torus evacuation system are transferred to a consolidation manifold. The gas mixture is then compressed to 0.1 MPa by a series of oil-free metal bellows pumps. The fuel is purified by trapping the condensible impurities at 30°K. The trapped impurities are processed to recover residual tritium by hot gettering or by a series of cryochemical separations [26]. Helium is removed by a cryogenic stripping column. The purified fuel is isotopically enriched by a cryogenic distillation cascade, [25] then prepared for delivery to the torus as ambient gas, frozen pellets or neutral beams.

Every effort is made to minimize the likelihood and consequences of leaks. The tritium handling components and hardware are enclosed in dry

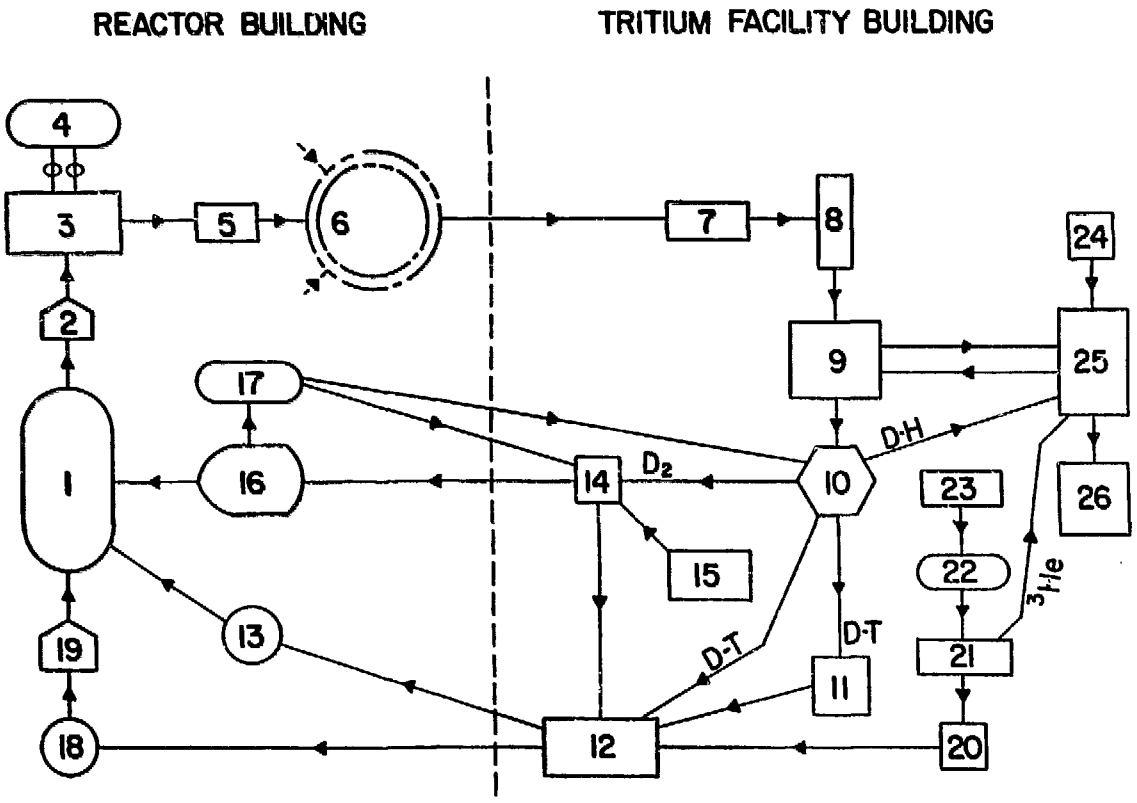

1. TORUS
2. DEBRIS SEPARATOR
3. VACUUM PUMPS
4. SAFETY SURGE TANK
5. REGENERATION PUMPS
6. CONSOLIDATION MANIFOLD
7. TRANSFER PUMPS
8. COMPRESSOR
9. IMPURITY REMOVAL
10. ISOTOPIC ENRICHMENT
11. D-T STORAGE
12. FUEL BLENDER
13. COLD FUEL INJECTOR
14. D_2 STORAGE
15. D_2 SUPPLY
16. NEUTRAL BEAM INJECTOR
17. BEAM PUMPING SYSTEM
18. FUEL LIQUIFIER
19. PELLET INJECTOR
20. T_2 RECEIVER/STORAGE
21. HELIUM REMOVAL
22. HOLDING TANK
23. T_2 SUPPLY HOOKUP
24. PURGE/EFFLUENT PROCESSING
25. WASTE CONSOLIDATION
26. WASTE DISPOSAL

Figure 8. Fuel Recycle Scenario for the ANL EPR Reactor.

gloveboxes or are jacketed in pipe casings. Further, the tritium processing components indicated in Figure 8 and the emergency air detritiation system are located in a separate, reinforced containment building. The jacketing pipes and gloveboxes are purged with an inert gas stream which is processed by a tritium waste treatment system of the type described in Reference 26.

The total tritium inventory is $\sim$ 1300 g. Of this amount, the quantity ($\sim$ 130 g) that is present in the vacuum pumps and the fuel preparation units during normal operation could conceivably be released to the facility buildings (volume = 6×10^4 m^3). Should that quantity be accidentally released to the building, the 50 m^3/s emergency cleanup system would take about 50 hours to reduce the ambient tritium levels to recommended radiation control guidelines of 5 $\mu Ci/m^3$. A 1-cm thick steel membrane inhibits tritium escape through the walls of the containment building, in the event of a leak.

The principal parameters which characterize the tritium and vacuum systems are given in Table 12.

11. REACTOR FACILITY

The overall reactor facility is shown in Figure 9. It consists of the reactor building and seven major support buildings and structures. The reactor support facilities are located in an attached building adjacent to the main reactor cargo doors. This building houses the repair/maintenance hot cell, the mockup/test equipment and other special facilities for initial winding and cryostat preparation of the TF coils. Adequate cranes and access to equipment are provided for handling all reactor components prior to their installation. A third large structure also located adjacent to the reactor building houses the reactor magnet power supplies and compressors for the

Table 12. Tritium Facility and Vacuum Parameters

Toroidal Vacuum System				
Volume (m^3)		450		
Past-burn gas load ($Pa-m^3$)		490		
Dwell time (s)		15		
No. cryosorption pumps		12		
Speed/pump (m^3/s)		80		
Tritium Inventory				
Storage (30 days) (g)		1192		
Fuel preparation (g)		110		
Vacuum pumps (g)		20		
Total (g)		1344		
Mass Flow Rates	D	T	He	H
Cold gas load (g/day)	58	126		
Fuel makeup (g/day)	56	121		
Neutral beam injection (g/day)	51	---		
Exhaust (g/day)	138	207	53	2
Neutral beam exhaust (g/day)	99	3		

cryogenic units. Power leads are run through seals in the reactor containment to the various reactor components. An energy storage ring, remotely located, is part of the reactor power distribution system. The facility has a tritium facility for storage, preparation and reprocessing of reactor fuel and clean-up of tritium contamination. A 120-MWe power plant is a major facility feature. Other facility structures include an office building housing the control center, a waste heat cooling tower array and a 120 MWe power sub-station.

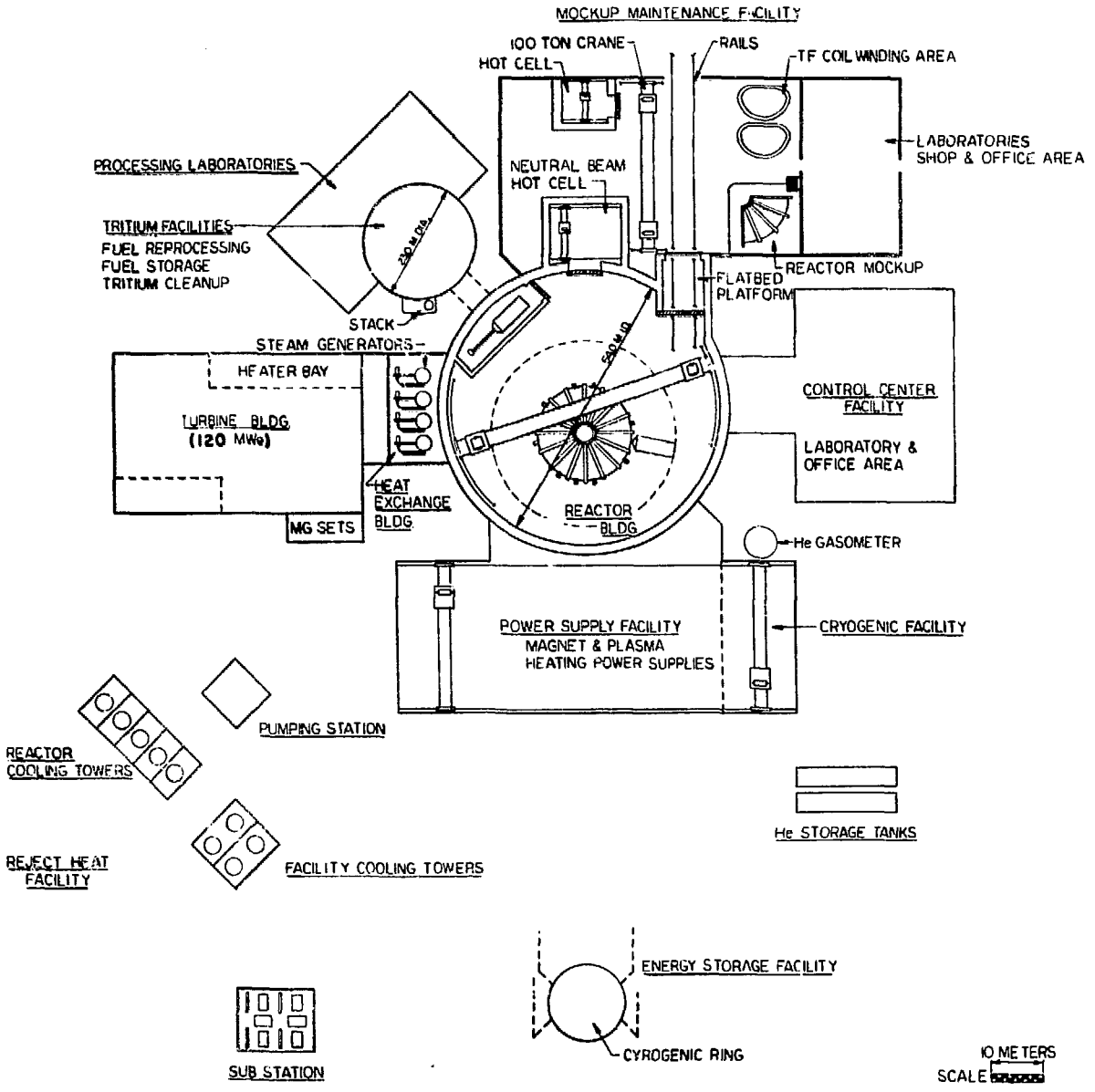

Figure 9. Plan View of Facility.

12. COSTS AND SCHEDULE

A cost estimate for EPR is given in Table 13.

A construction schedule from the beginning of site construction to initial startup is given in Figure 10. Several years of design would precede the beginning of site construction.

Table 13. Plant Capital Investment Direct Cost Estimate
(in millions of 1977 dollars)

1.0	Structures & Site Facilities	$ 46.0
2.0	Reactor	160.6
3.0	Reactor Plant Facilities	144.9
4.0	Turbine Plant	20.1
	TOTAL	$371.6
	Engineering (20%)	74.3
	Contingency (25%)	92.9
	GRAND TOTAL	$538.8

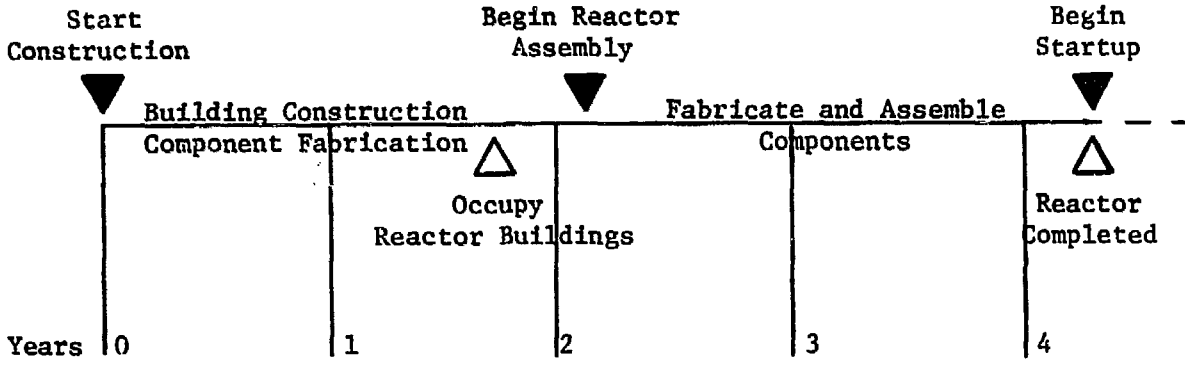

Figure 10. Reactor Construction Schedule.

REFERENCES

[1] STACEY, W. M., BAKER, C. C., ROBERTS, M., "Tokamak Experimental Power Reactor Studies," Presented at the Sixth International Conference on Plasma Physics and Controlled Nuclear Fusion Research, October 6-13, 1976, Berchtesgaden, Federal Republic of Germany; also, ERDA-76/139.

[2] STACEY, W. M., et al., "Tokamak Experimental Power Reactor Conceptual Design," Argonne National Laboratory, ANL/CTR-76-3 (August, 1976); and STACEY, W. M., et al., "Tokamak Experimental Power Reactor Studies," Argonne National Laboratory, ANL/CTR-75-2 (1975).

[3] "Experimental Power Reactor Conceptual Design Study," General Atomic Company, GA-A14000 (July, 1976); and "Experimental Power Reactor Conceptual Design Study," General Atomic Company, GA-A13534 (July, 1975).

[4] "Oak Ridge Tokamak Experimental Power Reactor Study," Oak Ridge National Laboratory, ORNL/TM-5572 through ORNL/TM-5577 (1976); and ROBERTS, M., BETTIS, E. S., "Oak Ridge Tokamak Experimental Power Reactor Study Reference Design," Oak Ridge National Laboratory, ORNL/TM-5042 (1975).

[5] CALLEN, J. D., DORY, R. A., "MHD Equilibria in Sharply Curved Axisymmetric Devices," Phys. Fluids, 5, 1523 (1972).

[6] PENG, Y-K., et al., "Magnetohydrodynamic Equilibria and Local Stability of Axisymmatic Tokamak Plasmas," Oak Ridge National Laboratory, ORNL/TM-5267 (1976).

[7] DORY, R. A., PENG, Y-K., "High-Pressure, Flux-Conserving Tokamak Equilibria," Oak Ridge National Laboratory, ORNL/TM-5555 (1976).

[8] EVANS, K., JR., "Magnetohydrodynamic Equilibrium Considerations in High-Beta Tokamaks," Argonne National Laboratory, to be published.

[9] EHST, D., EVANS, K., JR., STACEY, W. M., JR., "Tokamak Fusion Reactor Operating Regimes," Argonne National Laboratory, to be published.

[10] STACEY, W. M., JR., et al., "EPR-77: Revised Design for the okamak Experimental Power Reactor," Argonne National Laboratory, ANL/FPP/TM-77 (1977).

[11] GRIMM, R. C., et al., "Computation of the Magnetohydrodynamic Spectrum in Asixymmetric Toroidal Confinement Systems," J. of Comp. Phys., 16, 253 (1976).

[12] STACEY, W. M., JR., et al., "Impurity Control in Tokamak Reactors,", ANL/FPP/tm-91 (1977).

[13] PETERSON, H. A., et al., "Superconducting Inductor-Convertor Units for Pulsed Power Loads," Proceedings of the International Conference on Energy Storage, Conversion and Switching, November, 1972, Italy, Plenum Press, New York (1976).

[14] KUSTOM, R. L., et al., "The Use of Multiphase Inductor-Convertor Bridges as Actively Controlled Power Supplies for Tokamak EF Coils," Argonne National Laboratory, ANL/FPP/TM-78, to be published.

[15] PRAEG, W. F., "A Time-Delay Transformer for Overcurrent Protection", Record of the IEEE Power Electronics Specialists Conference, Cleveland, Ohio, June 8-10, 1976, p. 297-302.

[16] PRAEG, W. F., "A Power Supply for High Voltage Neutral Beam Injectors," Argonne National Laboratory, ANL/CTR/TM-67 (April 19, 1976).

[17] PRAEG, W. F., "Protection of Neutral Beam Accelerator Electrodes from Ore Discharges," Proceedings of the Seventh Symposium on Engineering Problems of Fusion Research, Knoxville, Tennessee (October 25-28, 1977), to be published.

[18] TURNER, L., WANG, S., SMITH, R., "Superconducting Magnet Systems for the ANL EPR Design," to be published as part of the Proceedings of the Seventh Symposium on Engineering Problems of Fusion Research, October, 1977.

[19] STEVENS, H. C., et al., "Tokamak Experimental Power Reactor Primary Energy Conversion System," Proceedings of the Second ANS Topical Meeting on the Technology of Controlled Nuclear Fusion, CONF-760935-P4 (1976), p. 1551.

[20] STEVENS, H. C., et al., "Mechanical Design and Analysis for an EPR First Wall/Blanket/Shield System", Proceedings of the Seventh Symposium on Engineering Problems of Fusion Research, Knoxville, Tennessee, October 25-28, 1977.

[21] MISRA, B., STEVENS, H. C., MARONI, V. A., "Thermal Hydraulic and Power Cycle Analysis for Near-Term Fusion Reactor Blanket Designs," Transactions of the American Nuclear Society 1977 Winter Meeting, November 22 - December 2, 1977, San Francisco, California.

[22] SMITH, D. L., CHARAK, I., "Thermal Response of Tokamak Fusion Reactor First Walls During Cyclic Plasma Burns," Proceedings of the Seventh Symposium on Engineering Problems of Fusion Research, Knoxville, Tennessee, October 25-28, 1977.

[23] YOUNGDAHL, C. K., MISRA, B., "Thermal Mechanical Design of Near-Term Fusion Reactor Blanket Blocks," Transactions of the American Nuclear Society 1977 Winter Meeting, November 22 - December 2, 1977, San Francisco, California.

[24] ABDOU, M. A., "Radiation Considerations for Superconducting Fusion Magnets," Argonne National Laboratory, ANL/FPP/TM-92 (1976).

[25] MISRA, B., MARONI, V. A., "Isotopic Enrichment of Plasma Exhausts from Controlled Thermonuclear Reactors by Cryogenic Distillation," Nuclear Technology, (in press).

[26] ANDERSON, J. L., SHERMAN, R. H., "Tritium Systems Test Assembly: Design for Major Tritium Device Fabrication Review," Los Alamos Scientific Laboratory, LA-6855-P (1977).